A Local Magnitude Scale from Borehole Recordings with Site Correction of the Surface to Downhole

Tz-Shin Lai[1,2], Wei-An Chao[*,3,4,5] , and Yih-Min Wu[1,6,7]

Abstract

The Central Weather Bureau of Taiwan deployed 62 borehole seismic stations equipped with accelerometers and broadband seismometers by the end of 2018. Currently, a large number of earthquake records has been accumulated because of the high seismicity rate of Taiwan. These records can be used to detect microseismicity because the background seismic noise level is lower at downhole stations than surface stations. However, the magnitudes of the waveforms recorded by the downhole stations are lower than those of surface stations because of near-surface site effects. In Taiwan, local magnitude (M_L) determinations use an attenuation function derived from surface stations, and M_L will be underestimated if this attenuation function is used for downhole stations. Records of 14,653 earthquakes were used to determine site amplifications corresponding to site corrections of the surface to downhole. For all available earthquake–station pairs, a total of 5470 amplification factors satisfied condition of the incident angle less than 35°, which are used for further discussion in this work. The results reveal that amplification factors ranging from 1.11 to 6.07 can be used to describe site effects. These amplification factors are strongly correlated with V_{S30} (average shear-wave velocity for the top 30 m of strata). The amplification factor was used to revise station M_L for downhole accelerometer (denoted M_{LB}), and revised M_{LB} (M_{LBNEW}) was compared with M_L from the surface accelerometer (denoted M_{LS}). Results show that M_{LBNEW} and M_{LS} are similar. Using the derived site corrections of surface to downhole, the downhole seismograms can be used to directly determine M_L, especially for the borehole broadband waveforms, enhancing detection capabilities for microearthquakes and improving the Taiwanese earthquake catalog.

Introduction

The local magnitude (M_L) scale introduced by Richter (1935) is widely used to report earthquake magnitude not only for rapid earthquake reporting (Kanamori, 1983) but also for estimating the strength of ground shaking in frequency ranges relevant to engineering applications (Kanamori and Jennings, 1978). M_L is originally defined for southern California based on earthquake recordings of the Wood–Anderson torsion seismograph. The Central Weather Bureau (CWB) of Taiwan adopted the empirical attenuation function proposed by Shin (1993) for M_L calculations using recordings of the three-component short-period digital seismographs at surface stations of the CWB Seismic Network (CWBSN). Since 2012, the CWBSN has been upgraded with 24-bit analog-to-digital converters and on-site Global Positioning System timing system; this network is called CWBSN24. Guan et al. (2020) derived new empirical attenuation functions based on seismic records from CWBSN24, improving the reliability and accuracy of earthquake magnitude reported to the public.

Since borehole seismic arrays were first used in CWB in 2008 (Fig. 1a), a large number of high-quality seismic waveforms have been recorded, enabling studies of near-surface attenuation and velocity structures (Wang et al., 2016), seismic anisotropy (Chen et al., 2017), earthquake early warning systems (Huang et al., 2016), and site amplification (Lai, Mittal, et al., 2016; Kuo et al., 2018). After the 1995 Hyogoken-Nanbu earthquake, the National Research Institute for Earth Science and Disaster Prevention in Japan constructed a surface-downhole observation

1. Department of Geosciences, National Taiwan University, Taipei, Taiwan, https://orcid.org/0000-0003-4542-1741 (Y-MW); 2. Seismological Observation Center, Central Weather Bureau, Taipei, Taiwan; 3. Department of Civil Engineering, National Chiao Tung University, Hsinchu, Taiwan, https://orcid.org/0000-0002-3228-9107 (W-AC); 4. Department of Civil Engineering, National Yang Ming Chiao Tung University, Hsinchu, Taiwan; 5. Disaster Prevention and Water Environment Research Center, National Chiao Tung University, Hsinchu, Taiwan; 6. Institute of Earth Sciences, Academia Sinica, Taipei, Taiwan; 7. Research Center for Future Earth, National Taiwan University, Taipei, Taiwan

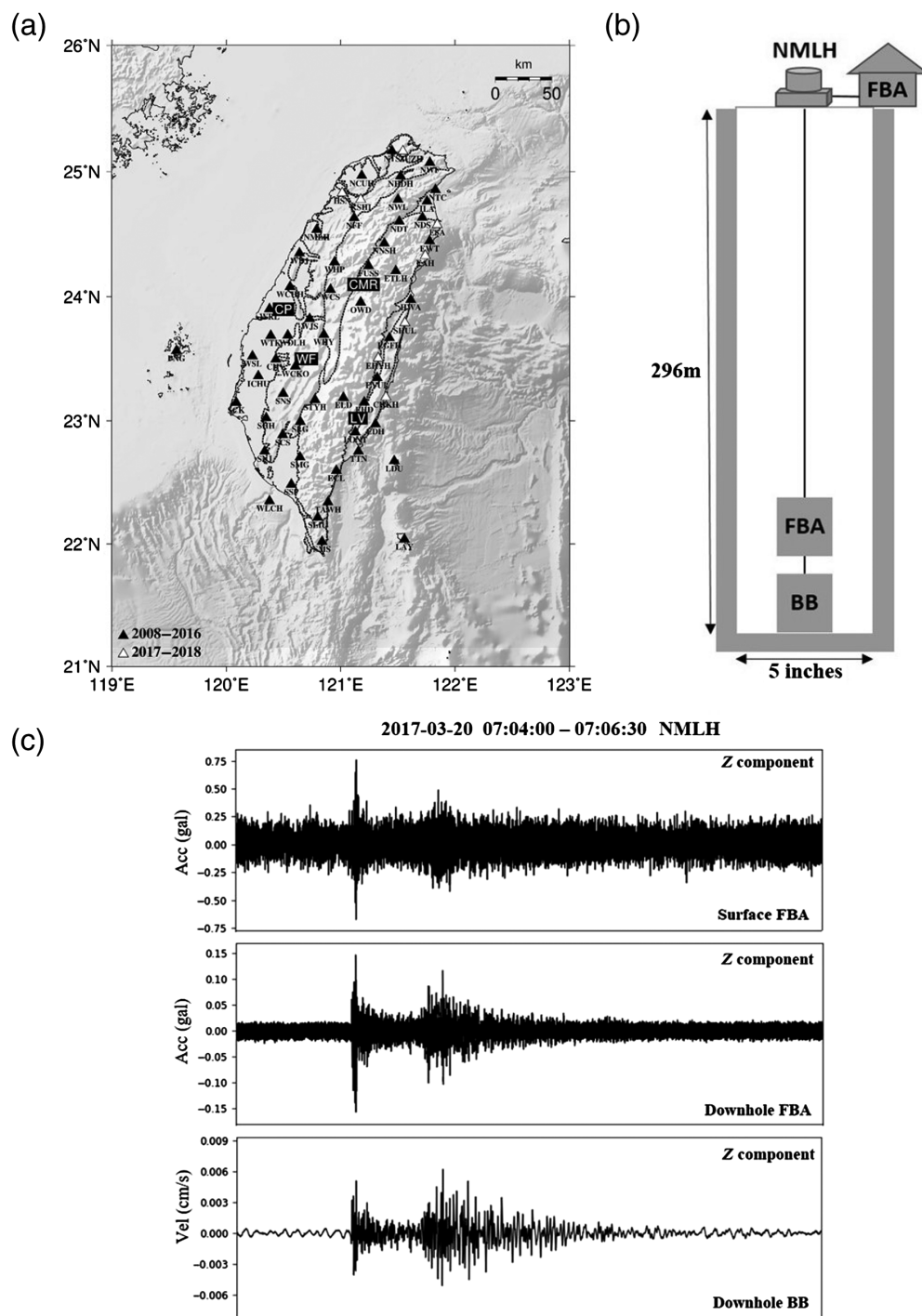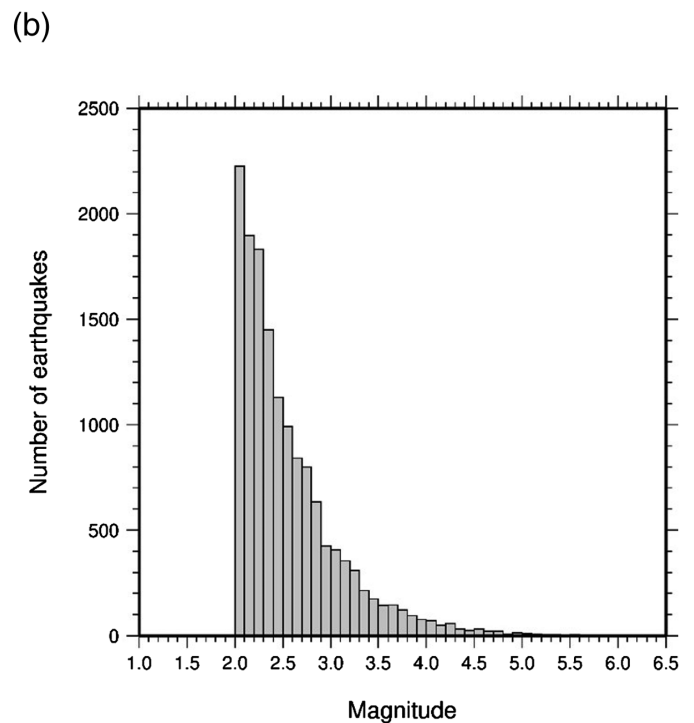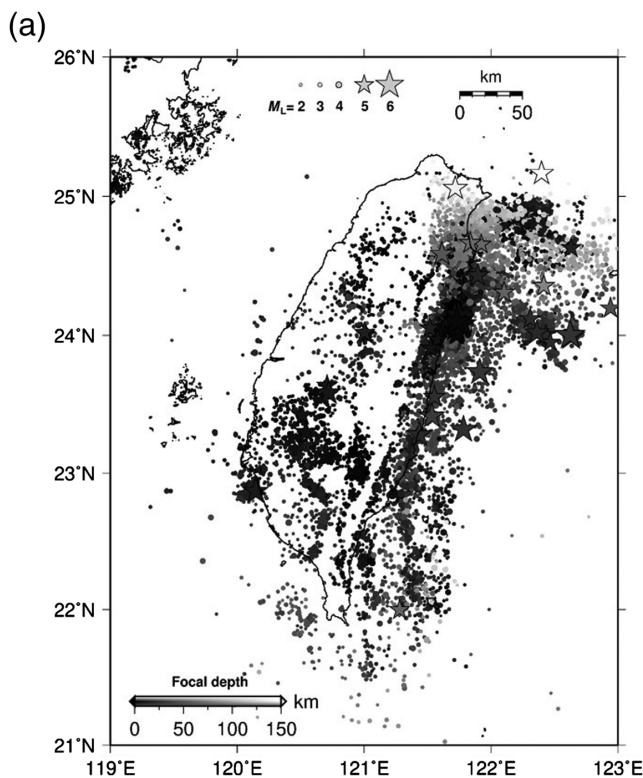*Corresponding author: wnchao@gmail.com; wnchao@nycu.edu.tw

Figure 1. (a) Distribution of the borehole seismic arrays in Taiwan. Black triangles represent 56 stations established between 2008 and 2016, and white triangles represent eight stations established between 2017 and 2018. Geological provinces are the Coastal Plain (CP), Western Foothills (WF), Central Mountain Range (CMR), Longitudinal Valley (LV). (b) The instrument configuration of the borehole seismic array at NMLH. FBA and BB represent the force balance accelerometers and broadband seismometer, respectively. (c) The seismic waveforms of the 20 March 2017, M_L 4.5 earthquake were recorded by the NMLH borehole seismic array at an epicentral distance of 136 km.

network, KiK-net (Aoi *et al.*, 2004). Several researchers have used spectral analysis of KiK-net database waveforms to assess near-surface site effects and site amplification factors (e.g., Oth *et al.*, 2011; Héloïse, Bard, and Rodriguez-Marek, 2012; Héloïse, Bard, *et al.*, 2012; Ibrahim *et al.*, 2014; Thabet, 2019). One advantage of borehole seismic arrays is enhanced microseismicity detection, facilitating the construction of a comprehensive earthquake catalog. However, the aforementioned site effect studies demonstrated that seismic amplitude was increased because of soft layers embedded in the subsurface. Consequently, earthquake-induced seismic amplitudes recorded by the downhole accelerometers are notably smaller than the surface recordings (Fig. 1b,c), resulting in underestimation of M_L scale when using the downhole recordings compared with surface station recordings. Therefore, the CWB's 62 downhole stations are not used to determine M_L for CWB earthquake reports. To use data from these stations, site corrections of surface to downhole must be derived for M_L estimation.

In this study, we first measured the site amplification factor (F) at each borehole array from the ratio of the peak amplitude of the simulated Wood–Anderson records from the surface and downhole strong-motion stations. Furthermore, F can be used as a site correction to revise single-station M_L scale using downhole recordings (M_{LB}). Discrepancies in M_L estimated from borehole and surface station data were investigated. We also compared near-surface

(a)

(b)

Figure 2. (a) Epicenter distribution of the 14,653 earthquakes occurring from 1 January 2017 to 31 December 2018 in Taiwan that were analyzed in this study. Sizes of the stars and circles are proportional to the magnitude, and colors represent ranges of focal depths. (b) Number of earthquakes as function of local magnitude.

site effects determined in the literature (Lai, Mittal, and Wu, 2016; Wen *et al.*, 2019) with the results of F. Finally, the seismic records of the borehole array for microearthquakes reported by Kuochen *et al.* (2019) were collected to examine the feasibility of M_L estimation from the borehole recordings using F-values for site correction. We also estimated M_L using the borehole broadband seismograms (M_{LB_BB}) and compared M_{LB_BB} with the M_{LB}. Borehole stations have high detection capability; therefore, the main goal of this study was to use the borehole recordings (broadband and strong-motion records) for estimation of M_L and to provide a more comprehensive earthquake catalog for advancement of seismological studies.

Data

To improve the regional monitoring capability of small-scale earthquakes in Taiwan, high-quality borehole seismic arrays have been under construction by the CWB since 2008. At the end of 2018, 62 borehole seismic arrays had been installed in Taiwan. Detailed information regarding the stations is presented in Table S1 available in the supplemental material to this article. The initial construction plan has been completed. Each borehole array includes two force balance accelerometers: one at the surface and another at a depth of 30–492 m. One broadband seismometer is located below the borehole accelerometer (Fig. 1b). The deepest downhole station is at station ICHU with the depth of 492 m, whereas the shallowest downhole is located at station ELD with the depth of 30 m. There are three types of instrumentation: (1) PA-23 accelerometers and KS-2000 broadband seismometers from Geotech, (2) CMG-5 T

accelerometers and CMG-3 TB broadband seismometers from Guralp, and (3) TitanPH accelerometers and Trillium 120PH broadband seismometers from Nanometrics (Table S1). The background seismic noise level is lower at downhole stations than at surface stations. Therefore, the seismic waveforms recorded by downhole stations are clearer than surface stations (Fig. 1c). The real-time continuous signals from the borehole seismic arrays are transmitted to the CWB seismological center. The sampling rate is 100 samples per second with 24-bit resolution. These borehole stations have the detailed drill core interpretations for identification of the lithological units.

The three-component seismic records of the borehole array from 14,653 earthquakes occurring between 1 January 2017 and 31 December 2018 are used in this study (Fig. 2a). These events, with the location quality levels A–C, satisfy the specific conditions of number of used stations (≥6), station gap (≤180°), and minimum epicentral distance (<50 km). During this data period, >56 borehole array stations were in operation in CWB. In our earthquake dataset, M_L ranges from 2.00 to 6.26 (Fig. 2b), and focal depths are between 1.0 and 270.2 km. For data preprocessing, these waveforms were

first corrected for baseline, demeaned, and detrended. Data containing unfavorable signals (e.g., data gaps caused by transmission problems) were removed. We only use the waveforms with signal-to-noise ratio (SNR) of >5 to study site corrections of surface to borehole.

Method

The formula for M_L (Gutenberg and Richter, 1956; Boore, 1989) is

$$M_L = \log A - \log A_0 + S, \tag{1}$$

in which A is the observed peak amplitude in mm, A_0 is the empirically determined distance correction, and S is the site correction. Richter (1935) defined M_L based on the peak horizontal amplitude recorded on a standard Wood–Anderson seismometer, and therefore the logarithm of A_0 would be -3 at a distance of 100 km away from the epicenter. In Taiwan, the attenuation function used to calculate M_L by the CWB was proposed by Shin (1993). For shallow earthquakes with focal depths ≤35 km,

$$\log A_0 = -0.00716R - \log R - 0.39(0 < \Delta \le 80 \text{ km}), \tag{2}$$

$$\log A_0 = -0.00261R - 0.83 \log R - 1.07(\Delta > 80 \text{ km}), \tag{3}$$

and for deep earthquakes with focal depths >35 km,

$$\log A_0 = -0.00326R - 0.83 \log R - 1.01, \tag{4}$$

in which Δ is epicentral distance and R is hypocentral distance. To investigate the differences in peak amplitude and determine the surface-to-borehole amplification factor, the accelerogram is simulated to Wood–Anderson record. In accordance with the official M_L estimation procedure of the CWB presented by Shin (1993), the horizontal peak amplitude (A_H) in millimeters from each station is determined by the root of sum of the squared peak amplitudes in the north–south (A_{NS}) and east–west (A_{EW}) components as presented in the following:

$$A_H = \sqrt{A_{NS}^2 + A_{EW}^2}. \tag{5}$$

We extracted A_H values from the surface (A_S) and downhole (A_B) horizontal seismograms for the purpose of estimating the surface-to-downhole amplification factor of (F), which can be used as the site correction term of the revised M_L scale. Here, we calculated the ratio of surface and borehole A_H values, denoted as the F-value:

$$F = A_S/A_B. \tag{6}$$

The station M_L values for surface stations (M_{LS}) and downhole stations (M_{LB}) are given by

$$M_{LS} = \log A_S - \log A_0, \tag{7}$$

$$M_{LB} = \log A_B - \log A_0, \tag{8}$$

in which A_0 is the distance correction, empirically determined using surface stations and ignoring the site correction term (Shin, 1993). Because of different site conditions of surface and downhole stations, the current attenuation function cannot be used to estimate M_L for downhole stations. Therefore, downhole stations have not been included for M_L determination by the CWB. The F-values determined in this study not only provide information regarding the site effects associated with the shallow layer but also can be applied to revise downhole station data, which is a direct way to correct the observed peak amplitude of borehole recordings and calculate M_L using the existed attenuation function. The revised station M_L for downhole accelerometer stations (M_{LBNEW}) is as follows:
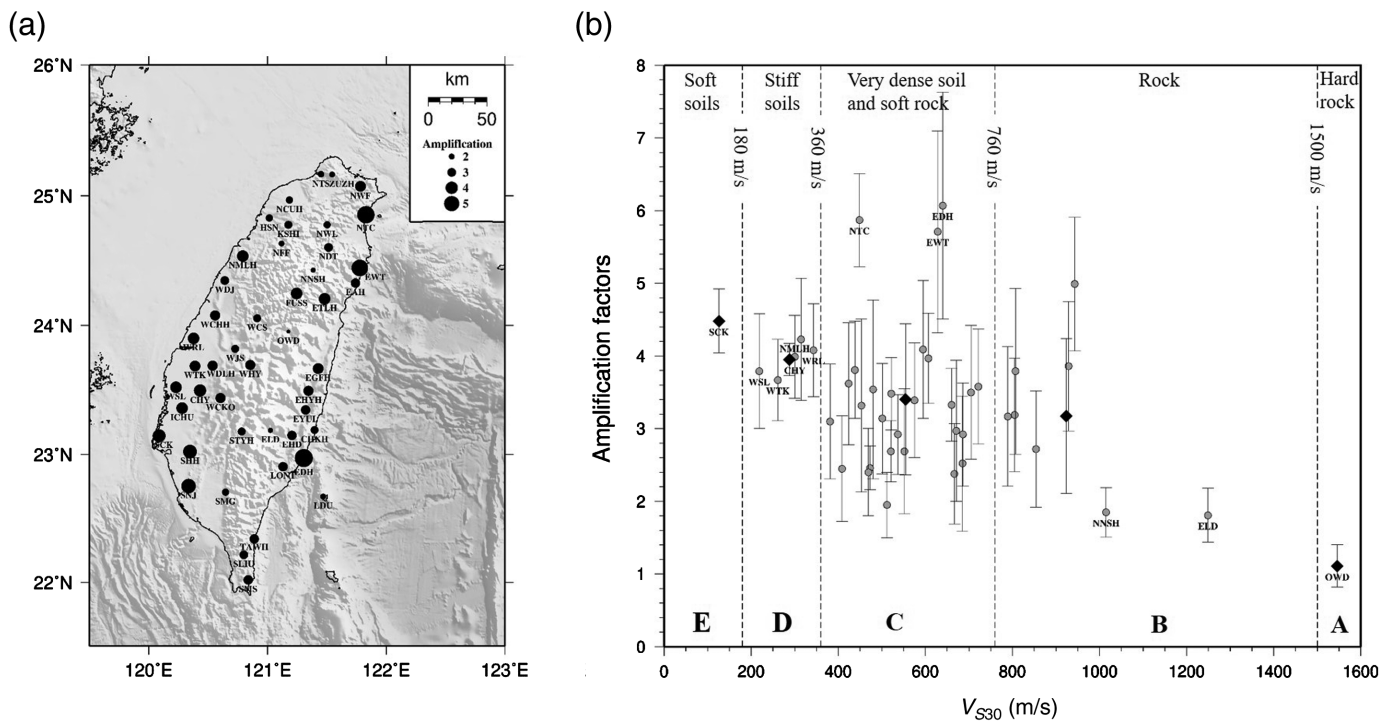
$$M_{LBNEW} = \log(A_B * F) - \log A_0 = \log A_B - \log A_0 + \log F$$
$$= \log A_B - \log A_0 + C, \tag{9}$$

in which C is the site correction of surface to downhole.

In fact, seismic wave horizontally incident on seismic borehole array can significantly influence the accuracy of the F-value. To avoid the aforementioned effect, we further adopt the 3D raytracing (Koketsu and Sekine, 1998) with the 3D velocity model of Wu et al. (2007) to calculate the incidence angle of each earthquake–station pairs and carefully examined the relationship between the incidence angle and the F-value for all available stations (Fig. S1). Finally, only results with incidence angles <35° were used in this study. The total number of F-values derived from the available earthquake–station pairs is 5470.

Results and Discussion

For each borehole seismic array, the F-value was calculated using equation (6) for each earthquake event. Table S1 displays the mean values of F with standard deviations. Figure 3a presents the distributions of the F-values, which range from 1.11 to 6.07. Overall, the F-value and geological setting of the region are strongly correlated. Smaller F-values of seismic stations in mountainous areas are determined. By contrast, higher F-values are determined of stations located in the western plains, which are rich in alluvium. The distribution of the F-values has a similar pattern to that of surface station M_L corrections (Lai, Mittal, and Wu, 2016). We further investigate the relationship between F-values and the average shear-wave velocity of the upper 30 m of a soil profile (V_{S30}). In Taiwan, V_{S30} is typically used for site classification (Lee and

Figure 3. (a) Distribution of the amplification factor (*F*) of borehole seismic arrays between surface and downhole stations. The sizes of the circles indicate *F*. (b) *F* as a function of V_{S30}. Labels A–E are the seismic site classifications. Gray dots represent *F* for each borehole seismic array, and black diamonds are the mean value at each classification with one standard deviation.

Tsai, 2008). V_{S30} for each borehole site was determined by Wen *et al.* (2019). They computed V_{S30} based on the V_S layer model derived from the receiver function of local earthquakes. Figure 3b presents the negative linear relationship between *F*-values and V_{S30}. We observe relatively smaller *F*-values of the stations at hard rock or rocky site (site classes A and B; $V_{S30} > 760$ m/s). By contrast, stations at soft soil or stiff soil sites (site classes D and E; $V_{S30} < 360$ m/s) have larger *F*-values. Because of discrepancies in the depths of the downhole stations and the materials of the drill cores, a few stations do not follow the linear trend; these stations are typically of site class C. For example, three stations (NTC, EWT, and EDH) close to eastern coastal areas have high *F*-values. From the data of drill cores (Fig. S2), unconsolidated layer thickness of >100 m at NTC and EWT can explain these high *F*-values. But the abnormal *F*-value at EDH is not explained by the unconsolidated layer thickness, and further investigation is required. Notably, another station EAH, also located in a coastal region, had a lower *F*-value than stations NTC, EWT, and EDH. The relatively shallow depth of the downhole instrument (Table S1) and the thinner unconsolidated layer (Fig. S2) may have contributed to this lower *F*-value. Overall, a strong correlation between the thickness of unconsolidated layer and *F*-value is observed. For instance, the unconsolidated layer thickness observe at stations NNSH and OWD is <20 m, and these stations have smaller *F*-values. By contrast, station SCK has an unconsolidated layer thickness of >300 m and obtains a larger *F*-value (Fig. S2).

A comparison of M_{LS} and M_{LB} in our earthquake dataset is presented in Figure 4a. The M_{LS} values are 1.13 times larger than the M_{LB} values, with a standard deviation of 0.26. By

applying the site correction of surface to downhole (*C*; equation 9) with M_{LB}, the ratio between M_{LBNEW} and M_{LS} is reduced to 1.0 (Fig. 4b). Thus, we could also determine the earthquake magnitude (M_{LB_BB}) using downhole broadband seismograms and then correct M_{LB_BB} using the *C* coefficients for each borehole station derived from the surface-to-downhole accelerograms to estimate the revised M_{LB_BB} (M_{LB_BBNEW}). The purpose of the downhole broadband seismometers is to improve the SNRs of seismic recordings, facilitating microearthquakes monitoring. This study confirmed that correction using the *C*-value is necessary for magnitude estimation using the borehole recordings (accelerograms and broadband seismograms). To test the accuracy of M_{LB_BBNEW}, we first examined the relationship between M_{LB} and the M_{LB_BB}. Figure 4c presents a comparison between M_{LB} and M_{LB_BB}, revealing a consistent 1:1 ratio. The seismic records of the borehole array for the microearthquakes reported by Kuochen *et al.* (2019) were collected. They deployed 70 temporary seismic stations equipped with 4.5 Hz geophones and Texan data recorders around Hualien City after the 2018 M_w 6.4 Hualien earthquake to detect the aftershock sequence. They also applied spectral analysis to determine the seismic moment (M_0) and the moment magnitude (M_w) of the
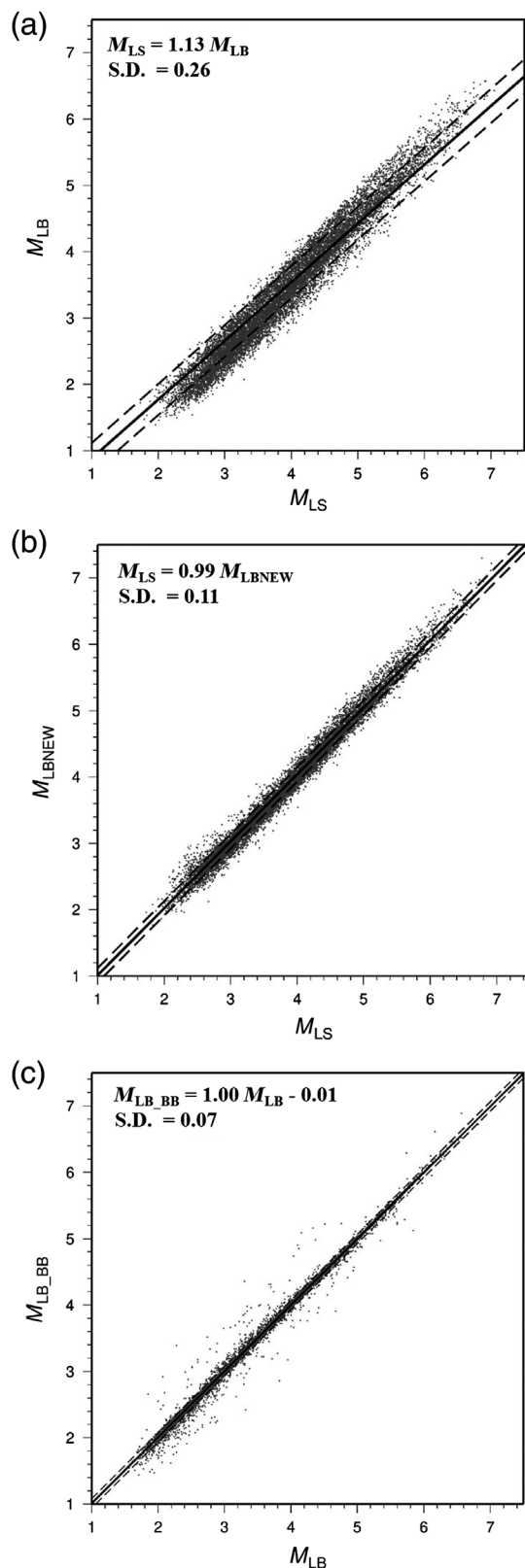
Figure 4. (a) Comparison of M_L as determined by surface stations (M_{LS}) or downhole station (M_{LB}). (b) After applying the site amplification factors to borehole stations, M_{LS} was compared with M_{LBNEW} by borehole stations. (c) Comparison of M_{LB} determined by FBAs or BBs. The solid line is the regression line with zero intercept; the two dashed lines indicate the standard deviation.

earthquake. For the 8 February 2018 earthquake listed in the catalog of Kuochen *et al.* (2019), the noise level of both the surface and downhole strong-motion stations (EAH; Table S1) was too high, and this earthquake cannot be detected (Fig. 5a). By contrast, the waveform recorded by the downhole broadband seismometer has a good SNR value and can be used for earthquake magnitude determination. Using the F-value of station EAH (3.14; Table S1), the station M_{LB_BB} of 1.62 can be corrected to be the M_{LB_BBNEW} of 2.12, consistent with the result of Kuochen *et al.* (2019) (M_w 2.2). For a moderate-sized earthquake (M_w 5.2) on 9 February 2018 reported by Kuochen *et al.* (2019), magnitudes determined in this study (M_{LS}, M_{LBNEW}, and M_{LB_BBNEW}) ranged from 4.81 to 4.85 and are between the real-time moment tensor (RMT) monitoring system solution (M_w 4.4; see Data and Resources) and the solution of Kuochen *et al.* (2019) (Fig. 5b). Different focal depths reported by earthquake catalogs may contribute to these discrepancies in magnitudes. The focal depths of the CWB earthquake report, the RMT solution, and Kuochen *et al.* (2019) were 5.82, 12, and 34.4 km, respectively.

Conclusions

In summary, the amplification factors (F) of peak amplitudes for surface-to-downhole site corrections (C) as derived in the present study successfully determined earthquake magnitudes using the borehole recordings (accelerogram: M_{LBNEW} and broadband seismogram: M_{LB_BBNEW}); the determined magnitudes are compatible with M_{LS}. Results reveal that the F-values for stations of site class A and B (e.g., NNSH, ELD, and OWD in Fig. 3b) were typically <2.0. By contrast, most stations of site class D or E (e.g., SCK, WSL, WTK, CHY, NMLH, and WRL in Fig. 3b) determined F-values of >3.5. Abnormal F-values for stations NTC and EWT of site class C can be explained by the thick unconsolidated layer beneath the stations (Fig. S2).

Using the calculated site corrections of surface to borehole (C), the downhole recordings can be used in CWB for earthquake monitoring, which will not only enhance location accuracy but also improve microseismicity detection capabilities.

Data and Resources

The seismic data used in this study can be found from the Geophysical Database Management System (GDMS; http://gdmsn.cwb.gov.tw, last accessed January 2022), Central Weather Bureau. The supplemental material for this article includes table list of the amplification factors (F) of borehole seismic array and figures displaying F-value as function of incidence angle and drill cores of borehole stations. Real-time moment tensor (RMT) monitoring system solution data are available at http://rmt.earth.sinica.edu.tw (last accessed May 2021).

Declaration of Competing Interests

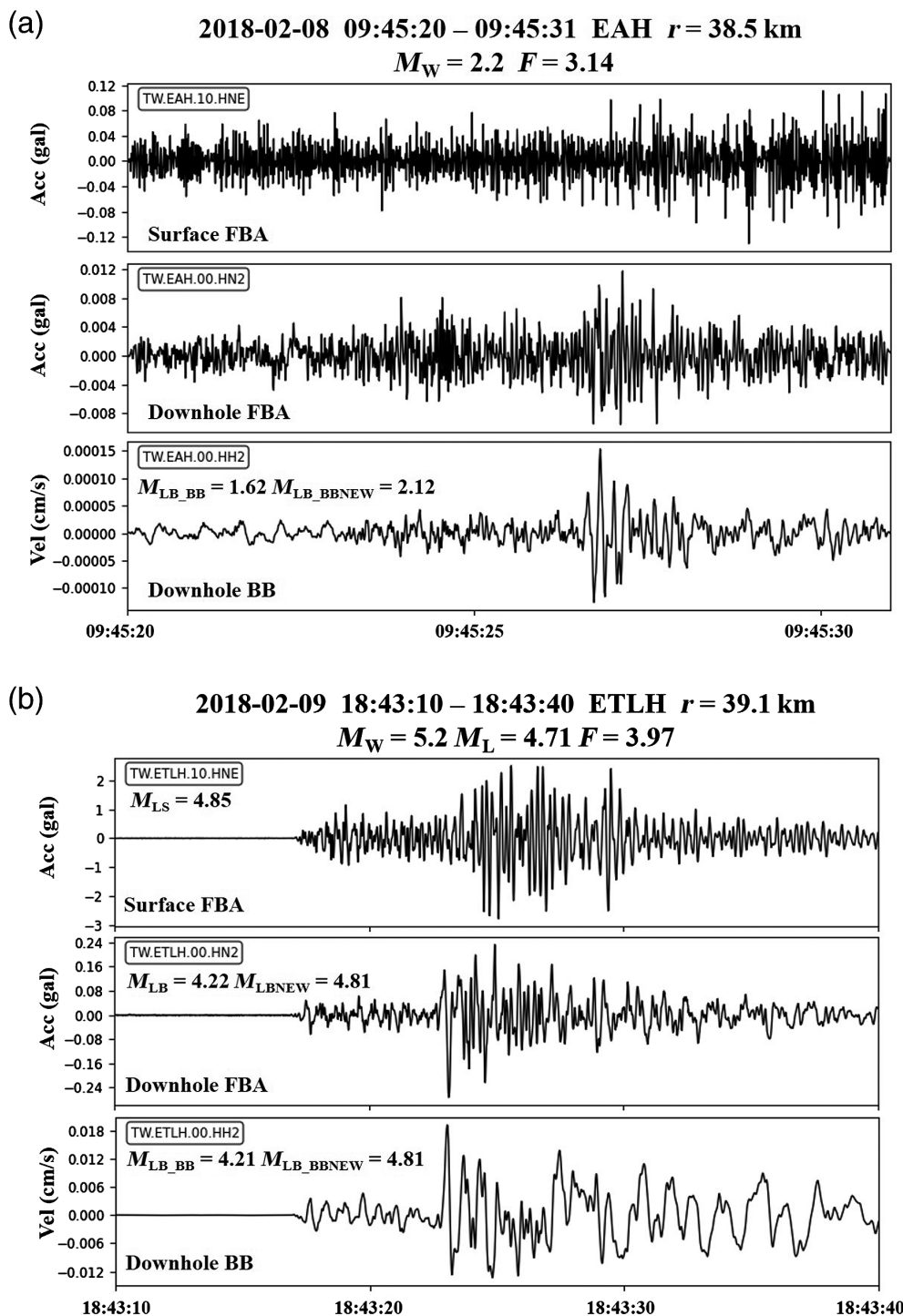The authors declare that there are no conflicts of interest.

Figure 5. (a) Seismic waveforms of the 8 February 2018 M_W 2.2 earthquake recorded by the EAH borehole seismic array. M_{LB} determined by downhole BB was 1.62, and M_{LBNEW} was 2.12 with site amplification factor 3.14 at station EAH with an epicentral distance of 38.5 km. (b) Seismic waveforms of the 9 February 2018 M_W 5.2 earthquake recorded by the ETLH borehole seismic array with an epicentral distance of 39.1 km. M_L was 4.71 according to the Central Weather Bureau earthquake catalog. At the ETLH surface station, M_{LS} was 4.85. M_{LB} determined by downhole force balance accelerometer (FBA) and BB were 4.22 and 4.21, respectively, and M_{LBNEW} was 4.81, close to M_{LS} after revision with site amplification factor 3.97.

References

Aoi, S., T. Kunugi, and H. Fujiwara (2004). Strong-motion seismograph network operated by NIED: K-NET and KiK-net, *Proc. Jpn. Assoc. Earthq. Eng.* **4,** 65–74.

Boore, D. M. (1989). The Richter scale: Its development and use for determining earthquake source parameters, *Tectonophysics* **166,** 1–14.

Chen, L. W., Y. N. Chen, Y. Gung, J. C. Lee, and W. T. Liang (2017). Strong near-surface seismic anisotropy of Taiwan revealed by coda interferometry, *Earth Planet. Sci. Lett.* **475,** 224–230.

Guan, Z. K., H. Kuo-Chen, and W. F. Sun (2020). Re-calculation of the attenuation functions for local magnitude from the upgraded Central Weather Bureau Seismic Network in Taiwan, *Terr. Atmos. Ocean. Sci.* **31,** 479–486.

Gutenberg, B., and C. F. Richter (1956). Earthquake magnitude, intensity, energy, and acceleration, *Bull. Seismol. Soc. Am.* **46,** 105–145.

Héloïse, C., P. Y. Bard, and A. Rodriguez-Marek (2012). Site effect assessment using KiK-net data: Part 1. A simple

correction procedure for surface/downhole spectral ratios, *Bull. Earthq. Eng.* **10,** 421–448.

Héloïse, C., P. Y. Bard, A. M. Duval, and E. Bertrand (2012). Site effect assessment using KiK-net data: Part 2—site amplification prediction equation based on f 0 and Vsz, *Bull. Earthq. Eng.* **10,** 451–489.

Huang, P. L., T. L. Lin, H. J. Hsiao, and R. H. Huang (2016). Taiwan borehole seismometer application in earthquake early warning, *Terr. Atmos. Ocean. Sci.* **27,** 819–824.

Ibrahim, R., H. Si, K. Koketsu, and H. Miyake (2014). Empirical spectral acceleration amplification in the Iwate–Miyagi and Niigata Regions, Japan, inferred by a spectral ratio method using ground-motion prediction equations, *Bull. Seismol. Soc. Am.* **104,** 1410–1429.

Kanamori, H. (1983). Magnitude scale and quantification of earthquakes, *Tectonophysics* **93,** 185–199.

Kanamori, H., and P. C. Jennings (1978). Determination of local magnitude, ML, from strong motion accelerograms, *Bull. Seismol. Soc. Am.* **68,** 471–485.

Koketsu, K., and S. Sekine (1998). Pseudo-bending method for three-dimensional seismic ray tracing in a spherical earth with discontinuities, *Geophys. J. Int.* **132,** no. 2, 339–346.

Kuo, C. H., K. L. Wen, C. M. Lin, N. C. Hsiao, and D. Y. Chen (2018). Site amplifications and the effect on local magnitude determination at stations of the surface–downhole network in Taiwan, *Soil Dynam. Earthq. Eng.* **104,** 106–116.

Kuochen, H., Z. K. Guan, W. F. Sun, P. Y. Jhong, and D. Brown (2019). Aftershock sequence of the 2018 Mw 6.4 Hualien earthquake in eastern Taiwan from a dense seismic array data set, *Seismol. Res. Lett.* **90,** 60–67.

Lai, T. S., H. Mittal, W. A. Chao, and Y. M. Wu (2016). A study on Kappa value in Taiwan using borehole and surface seismic array, *Bull. Seismol. Soc. Am.* **106,** 1509–1517.

Lai, T. S., H. Mittal, and Y. M. Wu (2016). 2012 Seismicity quiescence in Taiwan a result of site-effect artifacts, *Seismol. Res. Lett.* **87,** 848–852.

Lee, C. T., and B. R. Tsai (2008). Mapping Vs30 in Taiwan, *Terr. Atmos. Ocean. Sci.* **19,** 671–682.

Oth, A., S. Parolai, and D. Bindi (2011). Spectral analysis of K-NET and KiK-net data in Japan, Part I: database compilation and peculiarities, *Bull. Seismol. Soc. Am.* **101,** 652–666.

Richter, C. F. (1935). An instrumental earthquake magnitude scale, *Bull. Seismol. Soc. Am.* **25,** 1–32.

Shin, T. C. (1993). The calculation of local magnitude from the simulated Wood-Anderson seismograms of the short-period seismograms in the Taiwan area, *Terr. Atmos. Ocean. Sci.* **4,** 155–170.

Thabet, M. (2019). Site-specific relationships between bedrock depth and HVSR fundamental resonance frequency using KiK-NET data from Japan, *Pure Appl. Geophys.* **176,** 4809–4831.

Wang, Y. J., K. F. Ma, S. K. Wu, H. J. Hsu, and W. C. Hsiao (2016). Near-surface attenuation and velocity structures in Taiwan from wellhead and borehole recordings comparisons, *Terr. Atmos. Ocean. Sci.* **27,** 169–180.

Wen, K. L., C. H. Kuo, and C. J. Lyu (2019). Analysis of Vs profiles at CWB surface-downhole stations using receiver function of local earthquakes, *Central Weather Bureau Seismol. Center Tech. Rept.* 69 pp.

Wu, Y. M., C. H. Chang, L. Zhao, J. B. H. Shyu, Y. G. Chen, K. Sieh, and J. P. Avouac (2007). Seismic tomography of Taiwan: Improved constraints from a dense network of strong motion stations, *J. Geophys. Res.* **112,** no. B8, doi: 10.1029/2007JB004983.